ADVANCED FUNCTIONAL MATERIALS
www.afm-journal.de



# Restoring Intrinsic Properties of Electromagnetic Radiators Using Ultralightweight Integrated Metasurface Cloaks

*Zhi Hao Jiang, Peter E. Sieber, Lei Kang, and Douglas H. Werner**

**The concept of invisibility has garnered long-standing interest throughout human history but has only been realized experimentally within the past decade, albeit over a limited bandwidth. While the physical wave phenomenon of a reduced scattering signature has been demonstrated with different cloaking methods such as transformation optics and scattering cancellation, such technology has yet to be incorporated into any practical real-world devices. Through the use of quasi-2D functional metasurfaces, the long-standing issue of simultaneous mutual coupling and radiation blockage is addressed that occurs when two or more electromagnetic radiators are placed in close proximity to one another. The proposed compact and ultralightweight metasurfaces, comprising arrays of subwavelength electric and magnetic resonators with tailored dispersive properties, are capable of fully restoring the intrinsic properties of real-world electromagnetic radiators when placed in a multiradiator environment. This work introduces a general design approach to bridge the gap between the theory and practice for cloaks, which is applicable to microwave, terahertz, and optical radiators, as well as acoustic and thermal sources. Moreover, this technology provides an unprecedented opportunity for enabling high-density deployment of radiating systems with low interference and undistorted signal wave fronts.**

## 1. Introduction

Cloaks of invisibility and electromagnetic transparency have intrigued humans for centuries but realization of such devices has remained elusive until this past decade. With the recent advent of metamaterials,[1–4] a class of artificially engineered functional materials with exotic electromagnetic behaviors not present in natural materials, the concept of cloaking has emerged from the realm of imagination to become a physical reality. Over the past decade, various techniques have been proposed and subsequently demonstrated to achieve such physical phenomena under certain limitations throughout the electromagnetic spectrum.[5,6] The most well-known approach is based on transformation optics,[7–9] which exploits the form invariant properties of the Maxwell's equations under coordinate transformations.[4] While it is very difficult to realize an ideal spherical cloak due to the inhomogeneity and extreme anisotropy of the required material properties, several simplifications have been employed to facilitate realizable cloaks with small residual scattering. Such examples include the single polarization free space cloaks,[10,11] broadband carpet cloaks,[12–14] unidirectional and multiple directional cloaks,[15–18] broadband non-Euclidian cloaks,[19] surface-wave cloaks,[20] complementary medium cloaks,[21] and cloaks for DC electric or magnetic fields.[22,23] Scattering cancellation is an alternative approach where the dominant scattering terms present in the multipole expansion of the scattered fields are negated, greatly suppressing the overall scattering signature of an object.[6,24,25] In contrast to the complicated material properties required by transformation optics based cloaks, these coatings consisting of simple inhomogeneous and isotropic materials are sufficient to significantly reduce the scattered fields.[25–28] In the microwave and terahertz regimes, ultrathin metasurfaces can be used to replace bulk 3D metamaterial coatings for achieving the cloaking effect. This has been demonstrated to be effective for both dielectric and conducting objects, providing an ultralow-profile and lightweight alternative.[29–33] Apart from these two main categories of cloaking techniques, transmission-line networks and tapered parallel plates can also be utilized to achieve electromagnetic transparency.[34,35] At the same time, the concept of an invisibility cloak has also been extended to other realms of physics including acoustic cloaks,[36] thermal cloaks,[37–40] seismic cloaks,[41] and matter wave cloaks.[42] Despite these increasingly abundant examples of realizable cloaks, designs which incorporate this new technology into a real-world device have so far been elusive. While it has been suggested that cloaks could be used to create invisible receiving antennas and sensors,[43,44] demonstrations have only been reported for cylindrical obstacles placed in front of antennas[45] and sensors when operating in a receiving mode.[46]

As wireless technology continues to evolve at a rapid pace, a growing number of communication systems, each operating in a different frequency band, are being deployed on the same physical platform, resulting in significantly increased spatial

Dr. Z. H. Jiang, P. E. Sieber, Dr. L. Kang, Prof. D. H. Werner
Department of Electrical Engineering
The Pennsylvania State University
University Park
PA 16802, USA
E-mail: dhw@psu.edu

DOI: 10.1002/adfm.201501261

and spectral densities.[47] An immediate consequence is that multiple antennas, each one designed independently for a different system, are required to operate in close proximity to one another, inherently causing two correlated issues—mutual coupling (a near-field effect) and mutual radiation blockage (a far-field effect),[48] also referred to as "cosite interference."[49] Mutual coupling manifests itself when an electromagnetic wave from one radiator induces currents on another radiator, resulting in crosstalk and interference between the two systems. Additionally, mutual radiation blockage is attributed to the scattering of a radiated field due to the presence of additional radiators which, in turn, degrades the total radiation pattern. Recent efforts to reduce the mutual coupling effects in antenna systems have primarily focused on employing electromagnetic bandgap (EBG) materials to suppress bounded surface waves propagating in grounded dielectric substrates.[50,51] While these concepts are effective for microstrip and cavity-based planar radiators, they are not applicable for the more commonly used wire antennas where coupling occurs through unbounded waves propagating in free space. Single negative metamaterials have also been proposed to suppress the mutual coupling; however, due to the inherent impedance mismatch between the metamaterials and free space, the radiation wave front is still adversely impacted.[52] In order to compensate for mutual radiation blockage, transformation optics based cloaks have been proposed as a means of theoretically eliminating the performance degradation experienced when 2D radiators are placed in close proximity to each other.[53] However, for practical 3D radiators, the required material parameters involve inhomogeneity and extreme anisotropy. Hence, it would be exceedingly difficult to realize such complex coatings within the subwavelength volume required for most practical applications involving closely positioned sources. More recently, single-layer impedance surfaces that suppress the mutual blockage of wire radiators with ideal feeds have been reported and numerically validated.[54] While the proposed engineered surfaces are low profile and low loss, they often lead to stronger induced currents on the coated object, which in turn will produce stronger mutual coupling.[43,44,46] Thus, a single low-profile solution which simultaneously addresses both critical issues of mutual coupling and blockage does not currently exist. Such a technique, were it to be found, could have a profound impact by facilitating new possibilities in high density deployment of electromagnetic radiating systems, spanning from the microwave, through the terahertz, to possibly even the optical regimes. It may also pave the way for application to radiators in other physical forms such as acoustic transducers and thermal sources.

In this paper, for the first time, a unified approach is proposed which is capable of suppressing both the mutual coupling and mutual blockage caused by closely spaced real-world electromagnetic radiators using low-profile, ultralightweight integrated cloaking coatings. By tailoring the distinct anisotropic and dispersive properties of all metasurface layers comprising a composite coating, we demonstrate that the intrinsic properties of an enclosed radiator can be fully restored, operating as if there are no other radiators nearby. Based on the 2D theoretical analysis, the functional metasurface coatings, which are realized by arrays of subwavelength composite electric and magnetic unit cells, are designed and integrated with 3D monopole radiators. Both single-band and dual-band metasurface coatings are implemented, experimentally demonstrating practical cloaked electromagnetic radiators exhibiting not only greatly reduced mutual coupling but also near fully restored isotropic radiation patterns.

## 2. Restoration of Electromagnetic Radiator Properties Using Metasurfaces

The concept of simultaneous reduction of mutual coupling and mutual blockage between electromagnetic radiators is illustrated in **Figure 1**. Without loss of generality, we approach this problem by considering two conducting cylindrical electromagnetic radiators ($R_1$ and $R_2$), each emitting azimuthally omnidirectional waves into the surrounding free space, with $R_1$ and $R_2$ radiating at frequencies $f_1$ and $f_2$, respectively. When the two bare radiators are in close proximity (see Figure 1a), the electromagnetic radiation from $R_1$ induces current on the surface of $R_2$ at $f_1$, resulting in mutual coupling. This induced current, denoted as $J_1$, reradiates into the surrounding space at $f_1$, resulting in a distorted radiation pattern for $R_1$. Moreover, the scattered field produced by $J_1$ on $R_2$ will further induce current on $R_1$ at $f_1$, which changes the input impedance of $R_1$, thereby degrading the overall efficiency of the radiator. The same process happens when $R_2$ is radiating at $f_2$. For radiators with a subwavelength distance between one another, the analytically calculated electric field ($E_z$) distribution due to the radiation from each source is depicted in Figure 1c. As expected, strong induced currents are present on the surface of each radiator at the operating frequency of the other source, creating a significant amount of mutual coupling. Simultaneously, the scattered fields, originated from these induced currents, distort the originally omnidirectional radiation pattern, resulting in a strong angularly dependent distribution of outgoing radiated energy. Specifically, the mutual blockage greatly reduces the signal flow in the forward direction and results in peaks/nulls in the adjacent directions, greatly affecting the signal coverage and causing undesired crosstalk and shadow regions.

In order to simultaneously reduce the induced currents on the radiators and recover the omnidirectional wave front, composite coatings formed by two concentric metasurface layers are employed. Conceptually, as shown in Figure 1b, the composite coating for $R_i$ ($i = 1, 2$) is transparent at $f_i$, whereas it has dual functionalities at $f_j$ ($j \neq i$)—isolating $R_i$ from the outside world and cloaking $R_i$ to make the entire coated radiator completely invisible to waves emitted from $R_j$. The first function prevents waves from passing through the coating and in turn prevents them from interacting with the central radiator. The second function directs the waves around the coating, allowing the waves to follow their original trajectories unaltered. It should be noted that, in theory, these two functionalities can also be achieved by a transformation optics based cloak coating. However, to implement the required bulk spatially varying anisotropic material properties within a subwavelength volume would prove extremely difficult when compared to the inherently low-profile scattering cancellation approach enabled by the ultrathin metasurface coatings. Due to the fact that the metasurface has a near-zero electric thickness and is made from nonmagnetic

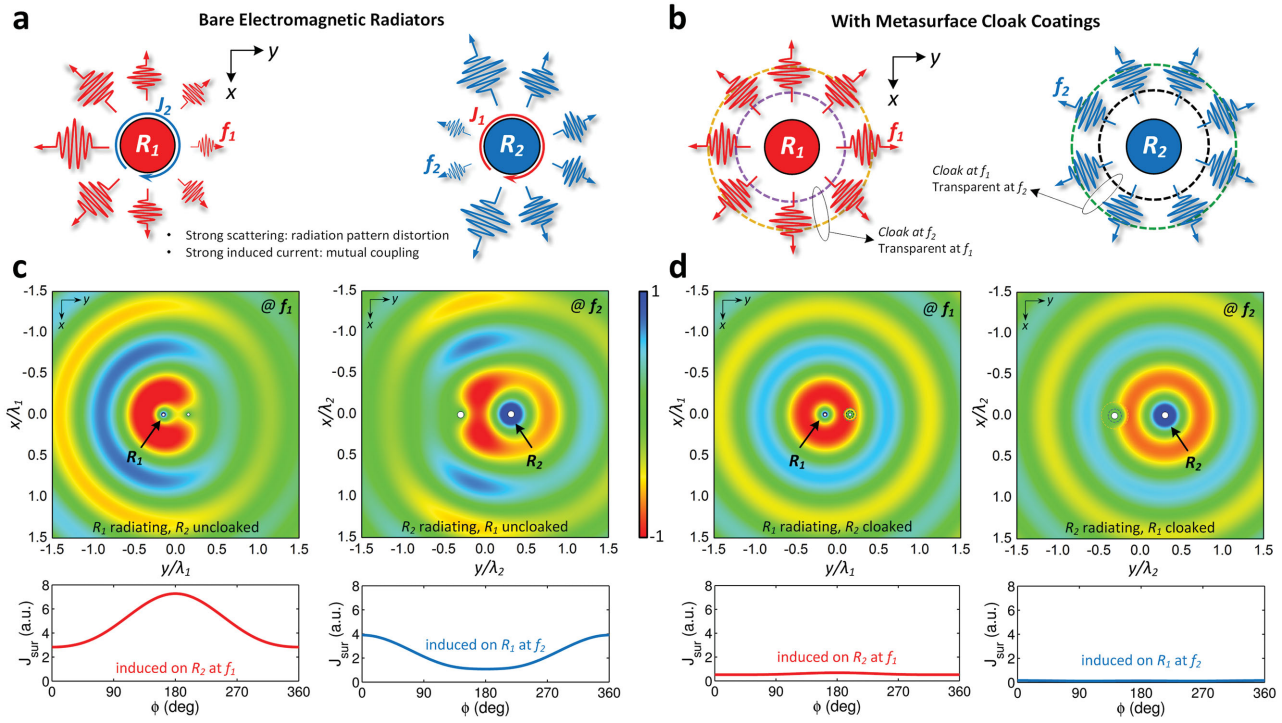


**Figure 1.** Functional metasurface coatings for restoring properties of electromagnetic radiators. a) Two bare closely spaced electromagnetic radiators operating at different frequencies induce current on each other due to mutual coupling and have distorted radiation patterns due to mutual blockage. b) Compact multilayer metasurface coatings with tailored dispersion enable near-zero induced current and recovered omnidirectional patterns for both radiators. c) Snapshots of the analytically calculated electric field distributions due to the radiation of each radiator, one at $f_1$ and the other at $f_2$ ($f_2 = 2f_1$), and corresponding induced current on the surface of the other radiator when both radiators are uncoated. The radius of the radiators is $0.02\lambda_1$ and the interradiator distance is $0.3\lambda_1$. d) Snapshots of the analytically calculated electric field distributions due to the radiation of each radiator and corresponding induced current on the surface of the other radiator when the metasurface coatings are present. At $f_2$, the inner metasurface for $R_1$ at a radius of $0.08\lambda_2$ has a $\alpha_{Ez}/\lambda_2 = 20$ and the outer metasurface at a radius of $0.16\lambda_2$ has a $\alpha_{Ez}/\lambda_2 = 0.3$ and a $\alpha_{M\rho}/\lambda_2 = -0.17$. At $f_1$, the inner metasurface of $R_2$ at a radius of $0.04\lambda_1$ has a $\alpha_{Ez}\lambda_1 = -20$ and the outer metasurface of $R_2$ at a radius of $0.08\lambda_1$ has a $\alpha_{Ez}\lambda_1 = 0.46$.

materials, its electromagnetic properties can be described by the surface electric and magnetic polarizability density tensors $\bar{\bar{\alpha}}_E = \mathrm{diag}\left[0, \alpha_{E\phi}, \alpha_{Ez}\right]$ and $\bar{\bar{\alpha}}_M = \mathrm{diag}\left[\alpha_{M\rho}, 0, 0\right]$.[55] The Mie scattering coefficients for all the modes under a cylindrical wave expansion and, in turn, the associated field distribution can be analytically calculated by solving the second order boundary conditions at both metasurface layers and the surface of the coated radiator (see the Supporting Information).[56,57] To achieve the two aforementioned goals simultaneously, the inner metasurface layer for each radiator is chosen to be either strongly capacitive or inductive. Consequently, this large shunt admittance results in a frequency-selective electromagnetic insulator. However, it also behaves as a strong scatterer as the induced currents are located at a larger radius, which deteriorates the radiation pattern of the nearby radiator. To mitigate this, an electrically complementary outer metasurface is utilized which cooperatively functions with the inner metasurface layer to minimize the scattering. The radii and the electrical properties of both metasurfaces are conjunctively tuned to enforce electromagnetic isolation between the inside and outside regions as well as a near-perfect cancellation of the dipole moments induced on the two metasurfaces and the central radiator.

The distributions of the analytically calculated electric field ($E_z$) radiated from each source, when integrated with the metasurfaces, are presented in Figure 1d. It can be seen that in contrast to the bare radiators, the metasurface coatings render the radiators invisible to the waves emitted from their neighboring elements. In addition to the recovered omnidirectional wave fronts, the total induced currents are reduced by more than one order of magnitude, directly corresponding to significant reduction in mutual coupling. While a single-layer metasurface can also achieve the cloaking effect, it does so at the expense of significantly increasing the induced currents (see Figure S2 in the Supporting Information). These 2D analytical results demonstrate the concept of using metasurfaces to simultaneously reduce both the mutual coupling and mutual blockage between multiple radiators operating at different frequencies, without adversely affecting their intended functionality. This method can be readily extended to the analysis of more general and complex cases where the number of radiators is greater than two and/or the number of nonoverlapping operational frequency bands of each radiator is greater than one.

## 3. Dispersive Metasurface Coatings for Practical 3D Radiators

To verify the concept proposed in the previous section, two quarter-wavelength monopole antennas fed by 50 Ω coax cables

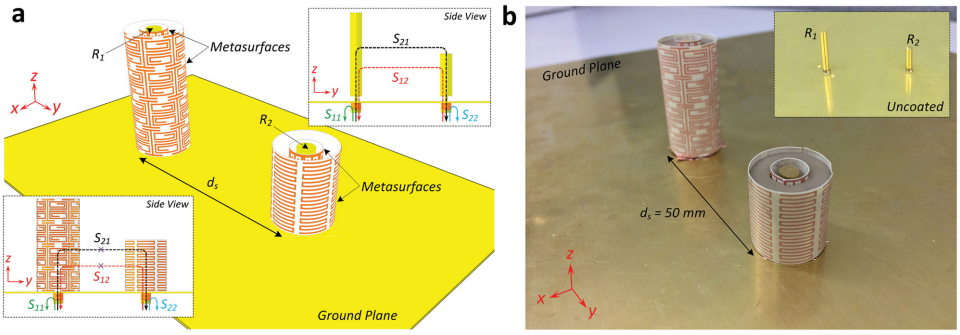


**Figure 2.** Functional metasurface coatings for real-world 3D monopole radiators. a) Configuration showing two metasurface cloaks used to coat a pair of 3D monopole radiators operating at 2.4 ($R_1$) and 5.2 ($R_2$) GHz, respectively. The ground plane size is 300 by 300 mm. The insets show the side view of the two radiator system with and without the metasurface coatings along with the notation used to define their associated S-parameters. The lengths of the two radiators $R_1$ and $R_2$ are 32 and 17.2 mm, respectively, for the case with coatings, while for the case without the coatings they are 29 and 15 mm, respectively. All the metasurfaces have six unit cells in the $\phi$-direction. b) A photograph of the fabricated monopole radiators coated by the assembled metasurface cloaks. The inset shows a photograph of the uncoated radiators.

are employed, which are commonly found in various wireless systems.[58] These vertical monopoles radiate signals omnidirectionally in the horizontal ($x$–$y$) plane into the surrounding free space, providing a 360° angular coverage. Although the operational frequencies of the two monopole radiators can be chosen arbitrarily, for this proof-of-concept demonstration they are selected to be 2.4 and 5.2 GHz which correspond to the wireless local area network (WLAN) bands used throughout the world. The configuration of the metasurface coated monopole radiators is shown in **Figure 2**a. The 2.4 GHz monopole $R_1$ and the 5.2 GHz monopole $R_2$, both with a radius of 2 mm, are positioned with a distance $d_s$ apart from each other on a finite sized ground plane. Each radiator is surrounded by a coating containing two finite concentric layers of ultrathin metasurfaces comprised of a finite array of periodic subwavelength anisotropic electric and/or magnetic resonators. The metallic patterns are printed on an ultrathin liquid crystal polymer dielectric substrate (Rogers Ultralam 3850) with a thickness of only 100 µm (<0.001$\lambda_0$ at 2.4 GHz). As the insets of Figure 2a show, without the coatings the two antennas interfere with each other as a result of mutual coupling. However, with the coatings, the magnitude of the transmission coefficient, characterized by $S_{21}$ (=$S_{12}$), can be greatly suppressed. The dispersive properties of the metasurface layers are jointly tailored to provide a maximal scattering reduction (i.e., cloaking) at the operational frequency of the other nearby radiator, while having a negligible impact on the input impedance of the enclosed radiator in its intended band of operation.

The unit cells of each metasurface layer for both radiators are shown in **Figure 3**a–d. During the unit cell design process, a finite element method solver, high frequency structure simulator (HFSS), was employed to perform the full-wave scattering calculations for a plane-wave at different angles of incidence. The relevant effective surface polarizability tensor parameters ($\alpha_{Ez}^{\text{eff}}$ and $\alpha_{M\rho}^{\text{eff}}$) were then retrieved from the complex reflection and transmission coefficients.[59] The radius values of the inner and outer metasurfaces for both radiators are 3.6 and 7.9 mm, which are only 0.029$\lambda_0$ and 0.063$\lambda_0$ at 2.4 GHz, respectively. For monopole $R_1$, the inner layer has a dispersive $\alpha_{Ez}^{\text{eff}}\lambda_0/\lambda_0$ with a near-zero value at its operational frequency of 2.4 GHz and a large value corresponding to the operational frequency of $R_2$, which is 5.2 GHz (see Figure 3a), indicating a strong capacitive response. This metasurface is therefore transparent at the operational frequency of $R_1$ and opaque at the working frequency of $R_2$. The outer metasurface of $R_1$ consists of a composite array of I-shaped electric resonators and broadside-coupled spiral magnetic resonators (see Figure 3b).[59] In order to work collectively with the inner metasurface to reduce the scattering caused by the coated monopole $R_1$ at the operational frequency of $R_2$, the values of $\alpha_{Ez}^{\text{eff}}/\lambda_0$ and $\alpha_{M\rho}^{\text{eff}}/\alpha_{M\rho}^{\text{eff}}\lambda_0$ were required to be 0.29 and –0.13, respectively, at around 5.2 GHz. They both have very small values at 2.4 GHz, which permits the near-perfect transmission of signals emitted from $R_1$. For the metasurface coating of monopole $R_2$, a similar design procedure can be adopted to control the dispersive response of each layer. The inner metasurface comprised of a meandered slot array has a near-zero $\alpha_{Ez}^{\text{eff}}/\lambda_0$ at around 5.2 GHz and a strongly inductive response at 2.4 GHz with a $\alpha_{Ez}^{\text{eff}}/\lambda_0 = -12$ (see Figure 3c). To collectively work with the inner metasurface for scattering reduction of $R_2$ at around 2.4 GHz, a second outer metasurface composed of an array of meandered dipoles[60] is included (see Figure 3d), which exhibits a Lorentzian-shaped electric response with $\alpha_{Ez}^{\text{eff}}/\lambda_0 = 0.47$ at 2.4 GHz and $\alpha_{Ez}^{\text{eff}}/\lambda_0 = -0.12$ at around 5.2 GHz. In contrast to the coating for $R_2$, the metasurface coating for $R_1$ requires a nonvanishing radial magnetic response to suppress the contribution of both the zeroth and first orders Mie scattering modes due to the fact that the size of its outer metasurface is beyond the quasi-static limit.[32,59] whereas the requirement on the radial magnetic response of the coating for $R_2$ can be relaxed.

## 4. Full-Wave Simulation Results of Coated Monopole Radiators

Once the metasurface designs were determined based on their responses in a 2D planar infinite array, finite versions of the structures were incorporated with the monopole radiators. The metasurfaces have an ultracompact subwavelength footprint, i.e., ≈0.013$\lambda^2_0$ at 2.4 GHz, and the same height as that of the

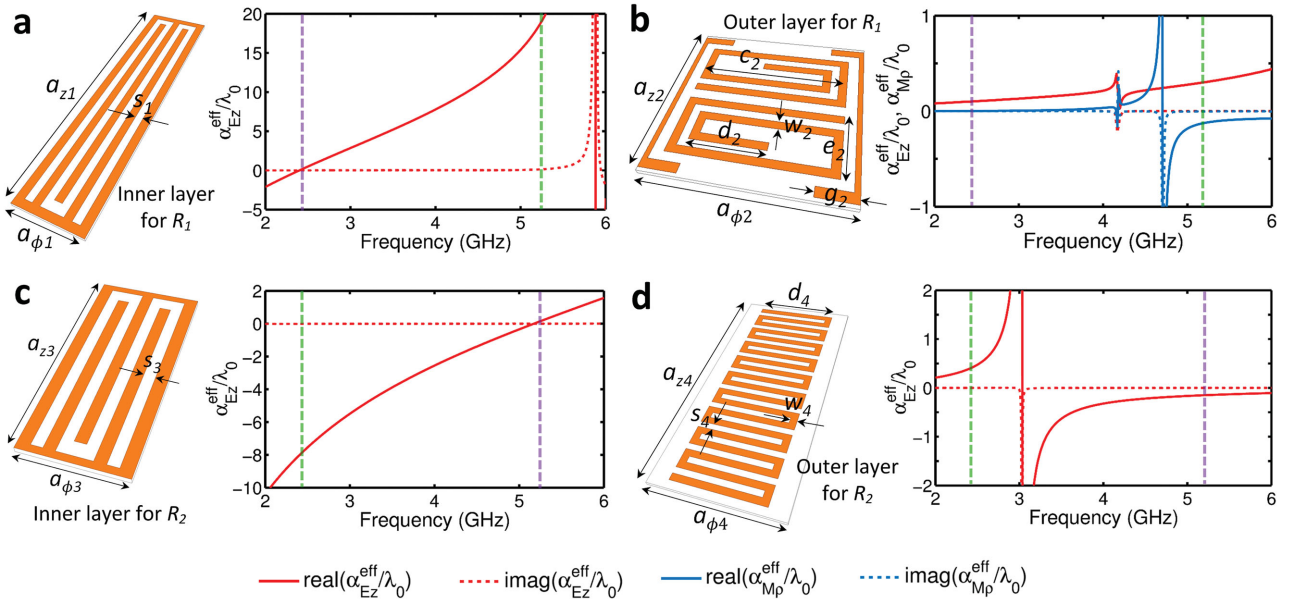


**Figure 3.** Unit cell and dispersive surface electromagnetic properties of the metasurface coatings. Configuration of the unit cells and retrieved effective surface electric and magnetic polarizability tensor parameters for a) the inner metasurface for radiator $R_1$, b) the outer metasurface for radiator $R_1$, c) the inner metasurface for radiator $R_2$, and d) the outer metasurface for radiator $R_2$. The geometrical dimensions are $a_{z1} = 16$, $a_{\phi1} = 3.77$, $s_1 = 0.4$, $a_{z2} = 8$, $a_{\phi2} = 8.27$, $c_2 = 6.5$, $d_2 = 2$, $e_2 = 2.6$, $g_2 = 2.5$, $w_2 = 0.35$, $a_{z3} = 8.6$, $a_{\phi3} = 3.77$, $s_3 = 0.4$, $a_{z4} = 17.2$, $a_{\phi4} = 8.27$, $d_2 = 6.2$, $s_4 = 0.54$,$w_4 = 0.33$, all in millimeters. The substrate material for all the metasurfaces is Rogers Ultralam 3850 ($\varepsilon_r = 2.9 - j0.007$) with a thickness of 100 μm.

corresponding monopole (see Figure 2a). In contrast to most of the previously demonstrated cloaks for infinitely long objects, here the geometrical dimensions of the metasurface unit cells were fine tuned to account for the truncation effect as well as the near-field coupling with the radiators, which jointly determine both the scattering reduction and impedance matching of the coated radiators.[61]

The full-wave simulated scattering parameters (S-parameters) of the two monopole radiators with and without the finite metasurface coatings are reported in **Figure 4**a,b. The center-to-center distance of the radiators is 50 mm. It can be observed that the transmission ($S_{21}$) between the two radiators is reduced by more than 25 dB around their operational frequencies, indicating a significantly suppressed mutual coupling down to around 0.3% of the level for the case without the coating. Additionally, an improved impedance matching is achieved for both monopole radiators at their operational frequencies; where $S_{11}$ decreases from −16 to −21 dB and $S_{22}$ drops from −13 to −18 dB, corresponding to reductions in the reflection loss by 68.4%.

The radiated power variation ($R_P$Var) in the $x$–$y$ plane of radiator $R_1$, quantified as the difference between the maximum and minimum gain values in the horizontal plane, i.e., max(gain, $\theta = 90°$) − min(gain, $\theta = 90°$), as a function of frequency is shown in Figure 4c. The $R_P$Var for the case where monopole $R_2$ is completely removed is also displayed as a reference. It can be seen that, when the coatings are present, the $R_P$Var of monopole $R_1$ is smaller than that of the case without the coatings within a range from 2.35 to 2.52 GHz. The best frequency is at 2.42 GHz, where the $R_P$Var drops from 32% down to only 8%, i.e., a relative reduction of 75%, which is almost the same as that of the monopole $R_1$ alone case, i.e., when $R_2$ is removed. These results indicate that the metasurface coatings are able to recover the wave front of the fields radiated from monopole $R_1$ by cloaking monopole $R_2$. The normalized radiation patterns in the $x$–$y$ plane of monopole $R_1$ operating at 2.42 GHz with and without the coatings are presented in Figure 4e. Improved omnidirectionality is observed, demonstrating that the scattering of the metasurface coated monopole $R_2$ is indeed considerably reduced. Simultaneously, the $R_P$Var of radiator $R_2$ in the $x$–$y$ plane is also greatly suppressed over a wide frequency range spanning from 4.78 to 5.57 GHz (see Figure 4d). At the optimal 5.22 GHz, the $R_P$Var drops from 63% to 18%, i.e., a relative reduction of 71%, which is only 9% higher than that of the monopole $R_2$ alone case, i.e., when $R_1$ is removed. At 5.22 GHz, the normalized radiation patterns in the $x$–$y$ plane of monopole $R_2$ with and without the coatings are presented in Figure 4f. Without the coatings, the patterns have two nulls at 20°/160° and exhibit a notably large contrast in the ±$y$-directions. With the coatings present, however, the nulls disappear and the radiation pattern becomes much more uniformly distributed. It should be emphasized that the antenna gain of $R_1$ and $R_2$ at their respective operational frequencies is well maintained at 4.7 and 5.5 dBi, respectively. In addition to the well matched input impedance, these results indicate that the metasurface coatings do not affect the radiation patterns produced by the monopole. The simultaneous suppression of both mutual coupling and mutual blockage is well maintained even when the center-to-center distance between the two radiators is reduced to 20 mm, i.e., $0.16\lambda_0$ at 2.4 GHz, further demonstrating the robustness of the proposed metasurface coatings (see Figure S3, Supporting Information).

To directly observe the cloaking effects as well as the reduced mutual coupling, especially in the near-field regions, the full-wave simulated electric field distributions on the

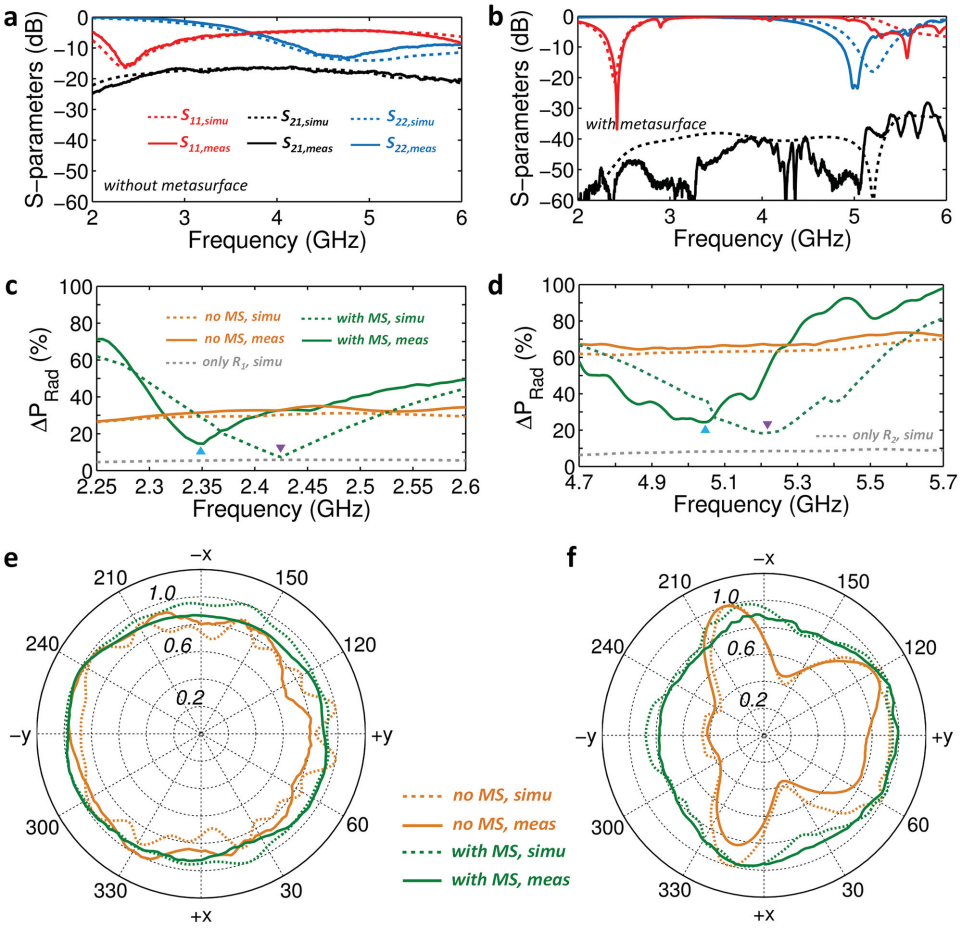


**Figure 4.** Simulation and measurement of 3D monopole radiator with and without metasurface coatings. Simulated and measured S-parameters a) without and b) with metasurface coatings. Simulated and measured radiated power variations of c) monopole $R_1$ and d) monopole $R_2$ in the $x$–$y$ plane as a function of frequency. Simulated and measured normalized radiation patterns of e) monopole $R_1$ and f) monopole $R_2$ in the $x$–$y$ plane.

ground plane at 2.42 and 5.2 GHz for the radiators with and without the metasurface coatings are reported in **Figure 5**. It can be seen from Figure 5a,b that, without the coatings, the wave front of the radiated fields produced by monopoles $R_1$ and $R_2$ are distorted as illustrated by the noncircular wave patterns. In contrast, when the monopole radiators are coated by the custom designed metasurfaces, the wave patterns on the ground plane are restored to concentric circles (see Figure 5c,d). Strong fields can be observed near the metasurfaces due to the presence of the discrete electric and/or magnetic resonators; however, the field strengths inside the inner metasurface are greatly reduced, verifying the low mutual coupling as previously indicated by the S-parameters. The recovered wave front in the near-field region demonstrates the possibility that radiators belonging to different systems can be successfully placed in close proximity to each other, without affecting their signal coverage or inducing intersystem crosstalk and interference. This allows for the placement of a greatly increased spatial density of systems on a single physical platform. Furthermore, the concept might also find application for reducing interference and coupling between compact on-chip nanoantennas or quantum emitters belonging to different subsystems.[62,63]

## 5. Experimental Verification

In order to demonstrate and subsequently validate the proposed design approach, the monopole radiators along with the custom designed metasurface coatings were fabricated and characterized. The flexible metasurfaces were first curled to form the concentric inner and outer layers. Next, thin Teflon washers were used as a frame to provide mechanical support and ensure correct diameters for both the inner and outer metasurface layers. The final fabricated ultralightweight coatings weighed less than 1 g. Photographs of the fabricated prototypes are displayed in Figure 2b. The measured S-parameters for the monopole radiators with and without the metasurface coatings were characterized by a network analyzer. The measured results are presented in Figure 4a,b which, except for a slight frequency shift of the coated monopole $R_2$ from 5.2 to 5 GHz, show very good agreement with simulation predictions. The measured $S_{11}$ and $S_{22}$ are both below −20 dB at the operational frequencies of $R_1$ and $R_2$, respectively, indicating a well-matched input impedance. The measured $S_{21}$ between the coated monopoles is about 30 dB lower than that of the uncoated monopoles, i.e., ≈0.1% of the level for the case without the coating. The radiation properties of

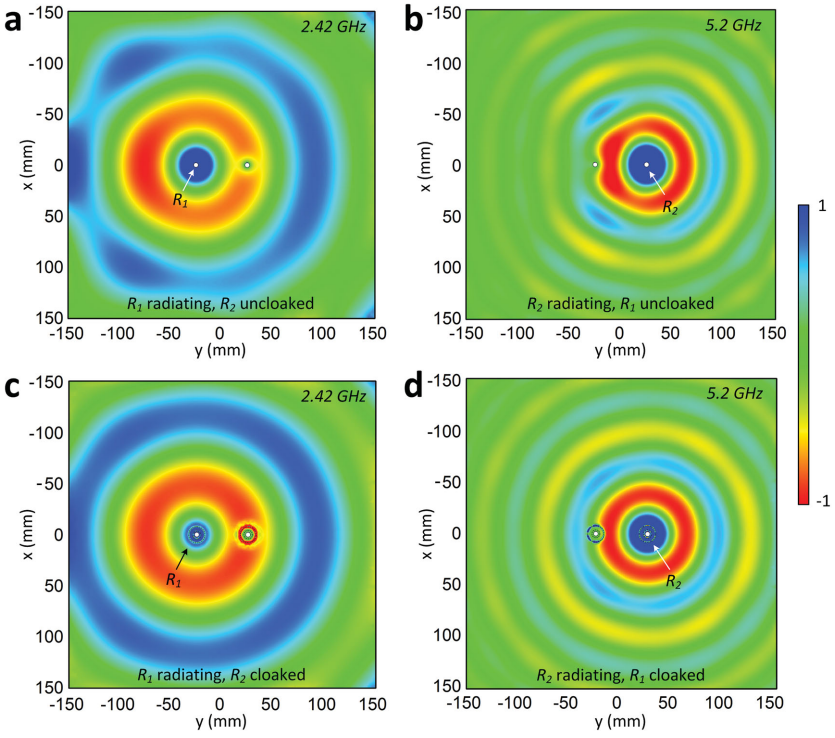


**Figure 5.** Full-wave simulated electric field distributions on the ground plane for the 3D monopole radiators with and without the metasurface coatings. Simulated electric field distributions on the ground plane when a) $R_1$ and b) $R_2$ is radiating, respectively, for the case without the metasurface coatings. Simulated electric field distributions on the ground plane when c) $R_1$ and d) $R_2$ is radiating, respectively, for the case with the metasurface coatings.

the monopole were characterized in an anechoic chamber. The measured $R_P$Var in the $x$–$y$ plane of radiator $R_1$ as a function of frequency is reported in Figure 4c, which exhibits a slight redshift due to fabrication imperfections. The smallest $R_P$Var is located at 2.35 GHz with a value of around 15%. The measured normalized radiation patterns at 2.35 GHz with and without the coatings are shown in Figure 4e, with increased radiation in the forward (+$y$) direction when the coatings are added. Similarly, for monopole $R_2$, the measured $R_P$Var also has a minor redshift which is again attributed to fabrication tolerances, with the lowest value of 23%, which is 5% higher than the simulated value, at 5.05 GHz (see Figure 4d). The measured normalized patterns of monopole $R_2$ for the cases with and without the coatings at 5.05 GHz are displayed in Figure 4f. The measured curves clearly show that the metasurface coatings are able to restore the onmidirectional characteristics of the patterns, corresponding well with the simulated patterns. The measured antenna gain values of $R_1$ and $R_2$ at their own operational frequencies are approximately 4.3 and 5.2 dBi, respectively, indicating a high radiation efficiency. In all, the experimental results confirm that the proposed metasurface coatings are capable of restoring the properties of practical 3D electromagnetic radiators when placed in close proximity by simultaneously suppressing both mutual coupling and mutual blockage effects.

## 6. Demonstration of a Multispectral Metasurface Cloaking Coating for Monopoles

As mentioned in the previous sections, the idea of cloaking practical electromagnetic radiators along with greatly reduced mutual coupling is not only effective for single-band sources but can also be extended to multi-band radiators. To demonstrate this, a dual-band metasurface coating was designed and fabricated to cloak a 2.4 GHz monopole radiator $R_1$ at two separate frequencies. As shown in **Figure 6**a, by only slightly increasing the overall footprint of the coated radiator, an additional third metasurface layer is employed to cloak the center monopole at both 3.5 and 5.2 GHz. The three layers are comprised of a meandered slot array, a composite I-shaped dipole and spiral resonator array, and a composite meandered dipole and I-shaped short dipole array, respectively (see Figure S4 in the Supporting Information). The geometrical dimensions of the resonators in each layer were optimized based on a similar design procedure as outlined previously by tailoring the values of the dispersive $\alpha_{Ez}^{eff}$ and $\alpha_{Mp}^{eff}$ to satisfy the requirements at 2.4, 3.5, and 5.2 GHz (see the Supporting Information). The overall footprint of the coatings is 8.6 mm which is only ≈9% larger than the previously demonstrated single-band coating. Next, an uncoated dual-band sleeve monopole radiator $R_2$, which radiates at 3.5 and 5.2 GHz, was placed at a distance of 50 mm away from $R_1$ for testing the effectiveness of the dual-band metasurface coating designed for $R_1$. The simulated S-parameters of the two radiators with and without the coatings are reported in Figure 6c,d. It can be seen that, without affecting the input impedance of the testing monopole $R_2$, the coating improves the impedance matching for $R_1$, showing a $S_{11}$ reduction from –15 to –21 dB. At around 3.5 and 5.2 GHz, the $S_{21}$ is reduced by 12 and 32 dB, respectively. Simultaneously, the $R_P$Var in the $x$–$y$ plane of radiator $R_2$ is also greatly suppressed in the frequency ranges from 3.29 to 3.64 GHz and from 4.82 to 5.47 GHz (see Figure 6e,f). At the best frequencies in each band, the $R_P$Var is reduced from 62% to 17% at 3.55 GHz and from 65% to 23% at 5.22 GHz. The normalized radiation patterns in the $x$–$y$ plane of $R_2$ for the cases with and without the coating at 3.55 and 5.22 GHz are displayed in Figure 6g,h, respectively. It can be seen that at 3.55 GHz, the coating transforms the bidirectional pattern into an omnidirectional pattern, while at 5.22 GHz, the tridirectional pattern becomes much more uniformly distributed.

The dual-band metasurface coating was fabricated, assembled, and characterized (see Figure 6b). The measured S-parameters of the monopole radiator with and without the coating are reported in Figure 6c,d, showing strong agreement with the simulated results. A reduction of more than 13 and

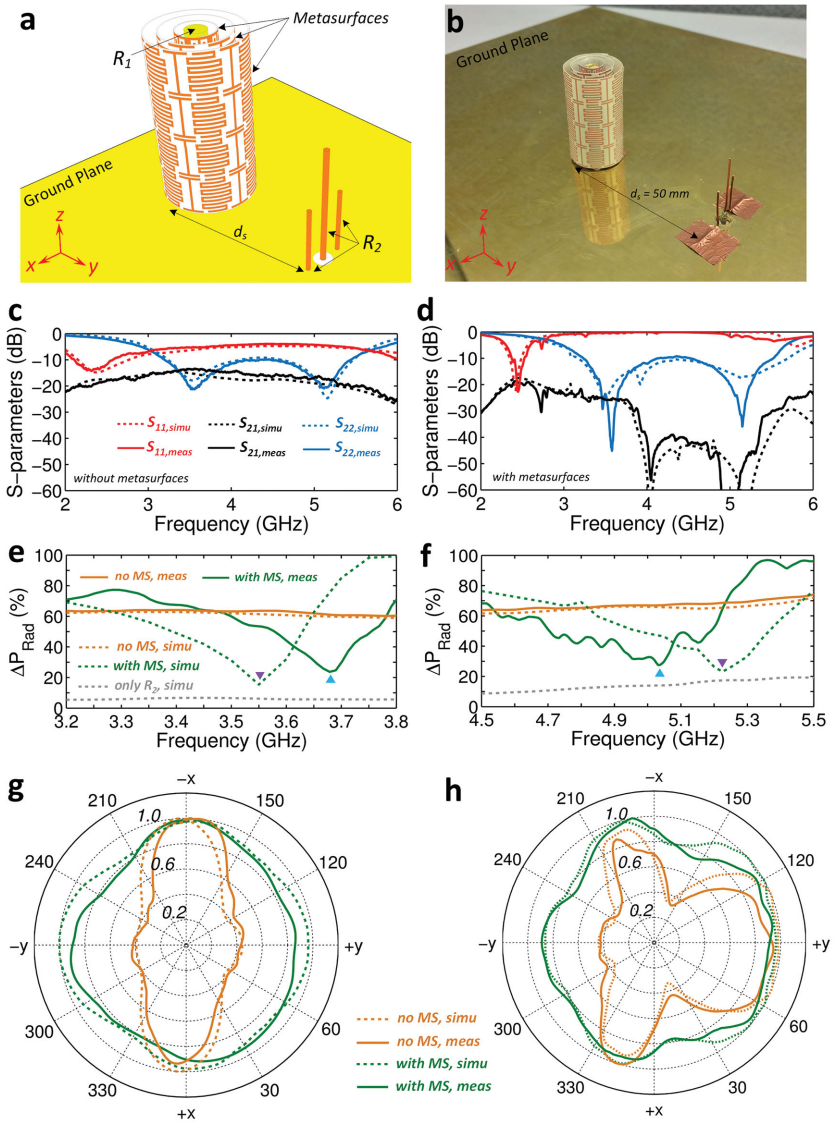


**Figure 6.** Dual-band metasurface cloak coating for 3D monopole radiator. a) Configuration of the dual-band metasurface cloak coated 3D monopole radiator ($R_1$) operating at 2.4 GHz. The testing antenna radiates at 3.5 and 5.2 GHz. The ground plane size is 300 by 300 mm. b) Photograph of the fabricated monopole radiator coated by the assembled metasurface cloak and the testing antenna. Simulated and measured S-parameters c) without and d) with metasurface coating. Simulated and measured radiated power variations of monopole $R_2$ in the $x$–$y$ plane at e) the lower band and f) the higher band. Simulated and measured normalized radiation patterns of monopole $R_2$ in the $x$–$y$ plane at g) the lower band and h) the higher band.

30 dB are achieved at the two radiating bands of $R_2$. The measured $R_P$Var in the $x$–$y$ plane of radiator $R_2$ in the first operational band is reported in Figure 6e, which shows a slight blueshift. The smallest measured value of $R_P$Var (around 22%) occurs at 3.68 GHz, which is only 3.6% higher than the simulation prediction, possibly due to the slight blueshift in the resonant frequency of the meandered dipole array. In the second operational band, the measured $R_P$Var in the $x$–$y$ plane of radiator $R_2$ is moved to the lower frequencies with its minimum at 5.04 GHz, which is 3.5% smaller than the best frequency predicted by the simulations (see Figure 6f). This is attributed primarily to the redshift in the resonant frequency of the fabricated spiral magnetic resonator array. Higher fabrication precision and more accurate assembly of the triple-layer coating should provide better agreement between simulation prediction and experimental results. The value of $R_P$Var at this minimum is around 27%, which is only 3% higher than the simulations predict. The measured normalized radiation patterns in the $x$–$y$ plane of $R_2$ for the cases with and without the coating at 3.68 and 5.04 GHz are displayed in Figure 6g,h, respectively. The measured patterns correspond well with the simulations, showing significantly improved uniform coverage of the radiated signal. This dual-band example further demonstrates that the proposed idea can be generalized to accomplish metasurface enabled cloaking coatings for practical electromagnetic radiators at multiple frequencies, while maintaining a compact footprint and an ultralightweight.

## 7. Conclusions

To summarize, a unified approach for restoring the intrinsic properties of electromagnetic radiators using compact and ultralightweight functional metasurface coatings was presented and experimentally demonstrated for the first time. It was demonstrated that by tailoring the dispersive properties of each metasurface layer of such coatings, the mutual coupling and mutual blockage between multiple radiators operating at multiple frequencies can be simultaneously reduced. Experiments performed on single-band and dual-band cloaking coatings for 3D electromagnetic monopole radiators have verified the proposed concept, confirming simultaneously suppressed mutual coupling and recovered radiation wave fronts. The resulting compact coatings, with a subwavelength footprint and ultralight weight (<1 g), will find potential applications in many types of microwave and millimeter-wave radiating systems. The general concept and design approach introduced here is expected to further pave the way for compact deployment of future on-chip terahertz/optical antennas as well as for a broader class of physical radiators including various acoustic and thermal sources.

## 8. Experimental Section

*Scattering Parameter and Radiation Pattern Measurement*: The scattering parameters of the two radiator system were measured by connecting the feed terminals of the two radiators to two corresponding ports of a network analyzer. The reflection magnitudes at each port

were recorded as $S_{11}$ and $S_{22}$, respectively, while the transmission magnitude was recorded as $S_{21}$, which is equal to $S_{12}$ due to reciprocity. The radiation patterns were measured in an anechoic chamber, where a standard horn antenna was used to transmit signals in the band of interest. Each radiator was used to receive the signal with the other radiator terminated by a matched load impedance of 50 Ω. The radiation pattern was obtained by recording the transmission amplitude between the horn and the radiator under test as the radiator was rotated in the horizontal plane, with a step size of 2°.

## Supporting Information

Supporting Information is available from the Wiley Online Library or from the author.

## Acknowledgements

This work was supported by a NSF MRSEC under Grant DMR-0820404.

Received: March 28, 2015
Revised: May 27, 2015
Published online: June 25, 2015

[1] G. V. Eleftheriades, K. G. Balmain, *Negative-Refraction Metamaterials: Fundamental Principles and Applications*, Wiley-IEEE Press, Hoboken, NJ **2005**.
[2] N. Engheta, R. Ziolkowski, *Metamaterials: Physics and Engineering Explorations*, Wiley-IEEE Press, Hoboken, NJ **2006**.
[3] T. J. Cui, D. R. Smith, R. Liu, *Metamaterials—Theory, Design, and Applications*, Springer, London, UK **2009**.
[4] D. H. Werner, D.-H. Kwon, *Transformation Electromagnetics and Metamaterials: Fundamental Principles and Applications*, Springer, London, UK **2014**.
[5] B. Zhang, *Light Sci. Appl.* **2012**, *1*, e32.
[6] P. Y. Chen, J. Soric, A. Alù, *Adv. Mater.* **2012**, *24*, 281.
[7] U. Leonhardt, *Science* **2006**, *312*, 1777.
[8] J. B. Pendry, D. Schurig, D. R. Smith, *Science* **2006**, *312*, 1780.
[9] D.-H. Kwon, D. H. Werner, *IEEE Antennas Proagat. Mag.* **2010**, *52*, 24.
[10] D. Schurig, J. J. Mock, B. J. Justice, S. A. Cummer, J. B. Pendry, A. F. Starr, D. R. Smith, *Science* **2006**, *314*, 977.
[11] W. Cai, U. K. Chettiar, A. V. Kildishev, V. M. Shalaev, *Nat. Photon.* **2007**, *1*, 224.
[12] R. Liu, C. Ji, J. J. Mock, J. Y. Chin, T. J. Cui, D. R. Smith, *Science* **2009**, *323*, 366.
[13] J. Valentine, J. Li, T. Zentgraf, G. Bartal, X. Zhang, *Nat. Mater.* **2009**, *8*, 568.
[14] H. F. Ma, T. J. Cui, *Nat. Commun.* **2010**, *1*, 21.
[15] B. Zhang, Y. Luo, X. Liu, G. Barbastathis, *Phys. Rev. Lett.* **2011**, *106*, 033901.
[16] X. Chen, Y. Luo, J. Zhang, K. Jiang, J. B. Pendry, S. Zhang, *Nat. Commun.* **2011**, *2*, 176.
[17] N. Landy, D. R. Smith, *Nat. Mater.* **2012**, *12*, 25.
[18] H. Chen, B. Zheng, L. Shen, H. Wang, X. Zhang, N. I. Zheludev, B. Zhang, *Nat. Commun.* **2013**, *4*, 2652.
[19] U. Leonhardt, T. Tyc, *Science* **2009**, *323*, 110.
[20] R. C. Mitchell-Thomas, T. M. McManus, O. Quevedo-Teruel, S. A. R. Horsley, Y. Hao, *Phys. Rev. Lett.* **2013**, *111*, 213901.
[21] F. Yang, Z. L. Mei, X. Y. Yang, T. Y. Jin, T. J. Cui, *Adv. Funct. Mater.* **2013**, *23*, 4306.
[22] S. Narayanan, Y. Sato, *Adv. Mater.* **2012**, *24*, 71.
[23] W. X. Jiang, C. Y. Luo, Z. L. Mei, T. J. Cui, *Appl. Phys. Lett.* **2013**, *102*, 140102.
[24] M. Kerker, *J. Opt. Soc. Am.* **1975**, *65*, 376.
[25] A. Alù, N. Engheta, *Phys. Rev. E* **2005**, *72*, 016623.
[26] C.-W. Qiu, X. Xu, Y. Feng, *Phys. Rev. E* **2009**, *79*, 047602.
[27] D. Rainwater, A. Kerkhoff, J. C. Soric, G. Moreno, A. Alù, *N. J. Phys.* **2012**, *14*, 013054.
[28] S. Xu, X. Cheng, S. Xi, R. Zhang, H. O. Moser, Z. Shen, Y. Xu, Z. Huang, X. Zhang, F. Yu, B. Zhang, H. Chen, *Phys. Rev. Lett.* **2012**, *109*, 223903.
[29] A. Alù, *Phys. Rev. B* **2009**, *80*, 245115.
[30] P. Y. Chen, A. Alù, *Phys. Rev. B* **2011**, *84*, 205110.
[31] J. C. Soric, P. Y. Chen, A. Kerkhoff, D. Rainwater, K. Melin, A. Alù, *N. J. Phys.* **2013**, *15*, 033037.
[32] Z. H. Jiang, D. H. Werner, *J. Phys. D: Appl. Phys.* **2013**, *46*, 505306.
[33] M. Selvanayagam, G. V. Eleftheriades, *Phys. Rev. X* **2013**, *3*, 041011.
[34] P. Alitalo, S. A. Tretyakov, *Proc. IEEE* **2011**, *99*,1646.
[35] S. Tretyakov, P. Alitalo, O. Luukkonen, C. Simovski, *Phys. Rev. Lett.* **2009**, *103*, 103905.
[36] L. Zigoneanu, B.-I. Popa, S. A. Cummer, *Nat. Mater.* **2014**, *13*, 352.
[37] R. Schittny, M. Kadic, S. Guenneau, M. Wegener, *Phys. Rev. Lett.* **2013**, *110*, 195901.
[38] S. Narayana, S. Savo, Y. Sato, *Appl. Phys. Lett.* **2013**, *102*, 201904.
[39] T. Han, X. Bai, D. Gao, J. T. L. Thong, B. Li, C.-W. Qiu, *Phys. Rev. Lett.* **2014**, *112*, 054302.
[40] H. Xu, X. Shi, F. Gao, H. Sun, B. Zhang, *Phys. Rev. Lett.* **2014**, *112*, 054301.
[41] S. Brûlé, E. H. Avelaud, S. Enoch, S. Guenneau, *Phys. Rev. Lett.* **2014**, *112*, 133901.
[42] S. Zhang, D. A. Genov, C. Sun, X. Zhang, *Phys. Rev. Lett.* **2008**, *100*, 123002.
[43] A. Alù, N. Engheta, *Phys. Rev. Lett.* **2008**, *102*, 233901.
[44] A. Alù, N. Engheta, *Metamaterials* **2010**, *4*, 153.
[45] J. Vehmas, P. Alitalo, S. Tretyakov, *IET Microw. Antennas Propag.* **2012**, *6*, 830.
[46] P. Fan, U. K. Chettiar, L. Cao, F. Afshinmanesh, N. Engheta, M. L. Brongersma, *Nat. Photon.* **2012**, *6*, 380.
[47] K. Slattery, H. Skinner, *Platform Interference in Wireless Systems—Models, Measurement, and Mitigation*, Elsevier, Amsterdam, The Netherlands **2008**.
[48] T. K. Sarkar, M. Salazar-Palma, E. L. Mokole, *Physics of Multiantenna Systems and Broadband Processing*, Wiley, Hoboken, NJ **2008**.
[49] D. Weston, *Electromagnetic Compatibility: Principles and Applications*, 2nd ed., CRC Press, Boca Raton, FL **2001**.
[50] D. F. Sievenpiper, L. Zhang, R. Broas, N. G. Alexopolous, E. Yablonovitch, *IEEE Trans. Microw. Theory Tech.* **1999**, *47*, 2059.
[51] F. Yang, Y. Rahmat-Samii, *IEEE Trans. Antennas Propagat.* **2003**, *51*, 2936.
[52] M. M. Bait-Suwailam, M. S. Boybay, O. M. Ramahi, *IEEE Trans. Antennas Propagat.* **2010**, *58*, 2894.
[53] D.-H. Kwon, D. H. Werner, *Appl. Phys. Lett.* **2008**, *92*, 113507.
[54] A. Monti, J. Soric, A. Alù, A. Toscano, L. Vegni, F. Bilotti, *IEEE Antennas Wireless Propagat. Lett.* **2012**, *11*, 1414.
[55] E. F. Kuester, M. A. Mohamed, C. L. Holloway, *IEEE Trans. Antennas Propag.* **2003**, *51*, 2641.
[56] T. B. A. Senior, *Appl. Sci. Res. B* **1960**, *8*, 418.
[57] W. C. Chew, *Waves and Fields in Inhomogeneous Media*, Wiley-IEEE Press, Hoboken, NJ **1999**.
[58] J. L. Volakis, *Antenna Engineering Handbook*, 4th ed., McGraw-Hill Professional, New York, NY **2007**.
[59] Z. H. Jiang, D. H. Werner, *Adv. Funct. Mater.* **2014**, *24*, 7728.
[60] Z. H. Jiang, Q. Wu, D. H. Werner, *Phys. Rev. B* **2012**, *86*, 125131.
[61] Z. H. Jiang, M. D. Gregory, D. H. Werner, *IEEE Antennas Wireless Propagat. Lett.* **2011**, *10*, 1543.
[62] J. Sun, E. Timurdogan, A. Yaacobi, E. S. Hosseini, M. R. Watts, *Nature* **2013**, *493*, 195.
[63] D. Dregely, K. Lindfors, M. Lippitz, E. Engheta, M. Totzack, H. Giessen, *Nat. Commun.* **2014**, *5*, 4354.